UCLA
COMPUTATIONAL AND APPLIED MATHEMATICS

Double Column Instabilities in the Barotropic Annulus

R.-Q. Lin

June 1988

CAM Report 88-19

Department of Mathematics
University of California, Los Angeles
Los Angeles, CA. 90024-1555

DOUBLE COLUMN INSTABILITIES IN THE BAROTROPIC ANNULUS.

R.-Q. Lin
Department of Mathematics
University of California
Los Angeles, California 90024

Received: June , 1988.

Abstract

The underlying reasons for the band structures seen in the atmospheres of Jupiter and Saturn are still incompletely understood. This paper gives quantitative support to a proposal made by Busse (1983), namely that the bands signal the presence of columnar convection rolls in the planetary atmospheres, such rolls being characteristic of convection in a highly rotating medium. It is necessary however to explain how such convection is capable of generating a striking characteristic of the planetary bands: the existence of a mean flow in the zonal direction that is in opposite directions relative to the surface of the planet in neighboring bands. This is the objective of this paper, the planetary atmosphere being for simplicity modeled by the barotropic annulus.

In the absence of mean flow, the columnar convection cells that intersect the surface of the planetary atmosphere in one latitude band, drift in longitude and have (as as a function of longitude) alternately one sense of vorticity and then the other. This paper simulates, through the barotropic annulus, convection in two adjacent latitude bands in a 'double column' structure. Initially, each band has an equal number of columnar convection cells of each sense of vorticity, and the mean zonal flow is small. It is shown that this arrangement is prone to a 'double column instability', in which the columnar cells of one sign of vorticity congregate in one of the latitude bands, those of the opposite sense of circulation gathering in the other. Associated with this redistribution of vorticity, a strong zonal motion develops. It is suggested that this provides a model for the zonal motion in a planetary band. The instability itself is the result of a resonance between two convective modes having almost equal zonal wavenumbers, the beat mode having a correspondingly large wavelength.

KEY WORDS: Thermal convection, barotropic annulus, Jupiter, Saturn

1. Motivation

This paper concerns the band structures seen on the faces of the major planets, Jupiter and Saturn. These have fascinated observers for centuries, and their origin has been one of the most tantalizing unsolved problem of the planetary sciences. Figure 1a shows a photograph of Jupiter, and next to it (Figure 1b) is a schematic diagram illustrating Busse's (1983) conception of the fluid motions that are responsible. From the Voyager flypasts, it is known that Jupiter's band structure is closely correlated with an alternation in the direction of zonal wind speed at the top of its atmosphere. Figure 2 shows this alternation, and also plots the East-West wind speeds; these range from +120m/s to -70m/s, approximately. There is, of course, no data available concerning the variation of wind speed with depth into its atmosphere, but Jupiter is so highly rotating that in all likelihood the motions are predominanly two-dimensional, with respect to the direction of the axis of planetary rotation, and such motions are sketched in Figure 1b. This does not explain how angular momentum is generated in alternating East-West directions in adjacent bands, but it is reasonable to suppose that convection processes are in some way responsible.

Two energy sources have been proposed. One relies on baroclinic and barotropic forcing and, as for the earth, derives its energy from solar heating; see Williams (1975, 1978, 1979a, 1979b, 1982, 1985). The other draws on sources internal to the planet, that set up a superadiabatic temperature gradient across the atmosphere which, if sufficiently great, allows convective instabilities; see Busse (1976, 1978). This paper adopts the Busse model for two reasons. First, observational data from Voyager 1 indicated that the temperature difference between the poles and equator of Jupiter is only 10% that of the Earth. Since the radius of Jupiter is about 10 times that of the Earth, the temperature gradient at the Jovian cloud tops is only 1% that found at the top of the Earth's atmosphere (Ingersoll, 1981). This suggests that baroclinic instabilities may be ineffective in mixing Jupiter's atmosphere. Second, the rate of infrared emission from Jupiter is roughly independent of latitude, and is greater than the rate of absorption of sunlight at all latitudes (Ingersoll, 1981). This indicates that the Jovian atmosphere is uniformly mixed, and also highlights the importance of heating from sources within the planet. Believing therefore that Williams's mechanism is the less effective of the two, we for clarity ignore it totally, and focus on Busse's proposal.

The first step in studying Busse's mechanism is to model the planetary atmosphere by a spherical shell that is uniformly heated from below or from within, and which is rapidly rotating. The effects of compressibility on the resulting convection are great but, when formulated in terms of the potential temperature and potential vorticity, the governing equations resemble those of Boussinesq convection, and give qualitatively similar results (Lin, 1988). We shall therefore employ the Boussinesq model throughout this paper.

Because of the constraints of rotation, marginal convection in a convecting Boussinesq sphere takes the form of thin "columnar vortices", or "thermal Rossby waves", aligned parallel to the axis of rotation. Because of the curvature of the sphere, these vortices are preferentially excited only at one particular distance from the polar axis of the planet. They intersect the surface of the sphere in two bands at the same preferred North and South latitudes, and are arranged symmetrically in longitude around that band, each

vortex rotating about its axis in the opposite sense to that of its two neighbors. This was demonstrated first in some detail by Roberts (1968) and later by Busse (1970), who also performed experiments that demonstrated the columnar structure of the convection (Busse, 1978). At larger convective amplitudes, vortices in adjacent latitude bands appear, being partially driven by the cells at the preferred latitudes, and being partially assisted by buoyancy forces. In this sequence of latitude bands, one sees the glimmerings of a mechanism that could explain the observations of Jupiter, but a serious obstacle remains: apparently the vortex system does not transport zonal angular momentum.

In marginal and near marginal conditions, the convective vortices that intersect the top of the atmosphere in one particular latitude band rotate alternately in opposite senses, and therefore transport zonal momentum alternately towards the East and towards the West. Averaged over longitude, the cancellation is complete, and no significant East-West flow is created. They are therefore incapable of accounting for the high zonal wind speeds shown in Fig. 2. Busse (1976) suggested however that, at a sufficient amplitude of convection, each vortex in one latitude band would pair with its partner in an adjacent band to form a double column, unstable to a process called "double-column instability". The final result of such an instability would, he supposed, be to cause vortices with one sense of rotation to congregate in one latitude band, while those of the opposite sense would congregate in adjacent latitude bands. In their new configuration, the mean zonal angular momentum flux would be considerable, and would create bands of alternating wind speed similar to those shown in Fig.2. The cells and associated bands conceived by Busse are sketched in Fig. 1b. The principal object of the present paper is to provide concrete evidence, for we believe the first time, that Busse's speculation is correct.

To demonstrate double-column instability, we follow Busse (1983) by simplifying the geometry. Instead of studying convection in a rotating sphere, or a rotating spherical shell, we shall study the very similar convection that arises in a rotating annulus, which has sloping ends and which is differentially heated from the sides (Fig. 3). The slope of the ends mimics the curvatures of the northern and southern hemispheres of the full sphere, and provides a model of convection in an equatorial band of Jupiter or Saturn's atmosphere. The fact that the preferred mode of convection in the full sphere takes the form of thin rolls implies that the geometry of the container outside these rolls, where the fluid is almost stagnant, should not much influence the nature of the convection in the rolls themselves. Thus, provided the side walls of the annulus are sufficiently separated, it should not matter that the full sphere has been limited in directions perpendicular to the rotation axis. The theory is, of course, rather easier to develop in the annulus than in the full sphere.

The present paper is a sequel to an earlier study of the annulus in which the author was involved (Lin *et al*, 1988), which was itself a sequel to an earlier paper by Or and Busse (1986). The former did not include the multiple longitudinal wave numbers needed to represent double-column instabilities [see (17) below]; the latter discarded the wave-wave interactions necessary to generate double-column instabilities. In the present paper, the necessary wave-wave interactions are included, and double-column solutions are obtained that, when they become unstable, reorganize themselves into structures of the kind conjectured by Busse. The expected enhancement in angular momentum flux results. In §2

the annulus model is defined, and a brief review of previous theoretical work is given. The governing equations and boundary conditions are set down, and the amplitude expansion method, that was used to solve the basic equations, is briefly reviewed. In §3 we describe the numerical results, and we exhibit the double-column instability explicitly.

2. The Annulus Model; Basic Equations; Mode Expansions

We consider convective flow in a cylindrical annulus cooled to temperature T_1 on its inside, heated to temperature T_2 on its outside, and rotating about the axis of symmetry, as shown in Figure 3; $\mathbf{\Omega}$ is its angular velocity. The slope of the top and bottom walls is $\tan^{-1}\eta_0$ and their mean separation is L. We use the gap width, D, between the cylindrical walls as lengthscale, D^2/ν as timescale, and $\nu\,\Delta T/\kappa$ as temperature scale. Here ν is the kinematic viscosity of the fluid, κ is its thermal diffusivity, and $\Delta T = T_2 - T_1$ is the temperature difference between the side walls. It is supposed that $D \ll r_0$, where r_0 is the mean radius of the annulus. In experiments, the acceleration due to gravity is small compared with the centrifugal acceleration $g = \Omega^2 r_0$ and may be neglected, i.e. gravity is effectively directed away from the rotation axis. In the planetary atmosphere, in which the annulus is meant to simulate an equatorial belt, the effective gravity is approximately directed towards the rotation axis, but the thermal forcing on the side walls is also reversed. The orthogonality of $\mathbf{g}$ and $\mathbf{\Omega}$ in the annulus therefore realistically models the approximate orthogonality of $\mathbf{g}$ and $\mathbf{\Omega}$ in the planetary belt.

Since $D \ll r_0$, the curvature of the annulus may be neglected, and Cartesian coordinates x, y, z may be set up that correspond respectively to distance from the center, O, of the fluid channel measured outwards away from the rotation axis, distance measured zonally round a line of latitude, and distance from O parallel to the axis of rotation. See Fig. 3.

Because the rotation rate is large, convection sets in as columnar vortices or thermal Rossby waves when the Rayleigh number,

$$R = \frac{\gamma\, g\, D^3 \Delta T}{\nu\,\kappa}, \tag{1}$$

exceeds a critical value, R_c, where γ is the coefficient of volume expansion. The convective flow is then nearly independent of z, and geostrophic balance almost holds, i.e.

$$\mathbf{v} = \boldsymbol{\nabla} \times [\psi(x, y, t)\,\mathbf{k}] + \mathbf{v}'(x, y, z, t), \tag{2}$$

where $\mathbf{k}$ is the unit vector parallel to $\mathbf{\Omega}$ and $\mathbf{v}'$ is the small ageostrophic part of the motion. The streamfunction ψ and the principal deviation, $\theta(x, y, t)$, of the temperature from the conduction solution (which is linear in x), satisfy

$$[\partial_t + \partial_y\psi\,\partial_x - \partial_x\psi\,\partial_y]\,\Delta_2\psi - \eta^*\partial_y\psi - \Delta_2^2\psi + R\,\partial_y\theta = 0, \tag{3a}$$

$$P\,[\partial_t + \partial_y\psi\,\partial_x - \partial_x\psi\,\partial_y]\,\theta + P\,\partial_y\psi - \Delta_2\theta = 0, \tag{3b}$$

Busse (1986). Here $\partial_t = \partial/\partial t$, $\partial_x = \partial/\partial x$ and $\partial_y = \partial/\partial y$; also Δ_2 $(= \partial_x^2 + \partial_y^2)$ is the two dimensional Laplacian, P $(= \nu/\kappa)$ is the Prandtl number, and

$$\eta^* = \frac{4\Omega D^3}{\nu L}\,\eta_0$$

is the scaled slope of the top and bottom of the annulus, and the term $\eta^* \partial_y \psi$ in (3a) arises from the application of the boundary conditions at those ends.

As Lin *et al* (1988) note, η^* is closely related to the familiar parameter β of dynamical meteorology. Though η_0 will be taken to be small, η^* will be assumed to be of order unity. In other words, we shall work with the double limit: $\eta_0 \to 0$, $\Omega D^3/\nu L \to \infty$, with $\eta^* = O(1)$. Even though $\eta_0 \ll 1$, we must assume that $\eta_0 \gg D/L$, in order to justify the neglect of Ekman pumping, in comparison with the geometrical effect of the sloping ends. The conditions on these boundaries need not be referred to again. The remaining boundary conditions, for the side walls, are

$$\psi = \partial_x^2 \psi = \theta = 0, \qquad \text{at} \qquad x = \pm \frac{1}{2}. \tag{4}$$

We shall concentrate on the case of large η^* as, in fact, Lin *et al* (1988) did.

When the amplitude of convection is infinitesimal, equations (3) are linear, and are satisfied by $\psi = \psi_0^{(n)}$, $\theta = \theta_0^{(n)}$ etc, where

$$\psi_0^{(n)} = \sin n\pi \left(x + \frac{1}{2} \right) e^{i(\alpha y + \omega t)}, \qquad \theta_0^{(n)} = \frac{i\alpha}{i\omega P + \alpha^2 + n^2\pi^2} \tilde{\psi}^{(n)}, \tag{5}$$

provided

$$\omega = \omega^{(n)} = -\frac{\alpha \eta^*}{(1+P)(\alpha^2 + n^2\pi^2)}, \tag{6a}$$

$$R = R^{(n)} = \frac{(\alpha^2 + n^2\pi^2)^3}{\alpha^2} + \left(\frac{\eta^* P}{1+P} \right)^2 \frac{1}{(\alpha^2 + n^2\pi^2)}. \tag{6b}$$

The critical case of minimum $R^{(n)}$ is distinguished by the subscript $_c$. It is found that, when η^*, or more precisely

$$\eta_p \equiv \frac{P}{\sqrt{2}(1+P)} \eta^*, \tag{7}$$

is large, $R^{(n)}$ is independent of n, provided $n \ll \eta_p^{1/3}$. To leading order for $\eta_p \to \infty$

$$\alpha_c^{(n)} \sim \eta_p{}^{\frac{1}{3}}, \qquad \omega_c^{(n)} \sim -\frac{\sqrt{2}}{P} \eta_p{}^{\frac{2}{3}}, \qquad R_c^{(n)} \sim 3\,\eta_p{}^{\frac{4}{3}}. \tag{8a, b, c}$$

At the next level of the large η_p expansion, small n-dependent terms appear. For $n\,\eta_p^{-1/3} \ll 1$,

$$\alpha_c^{(n)} \sim \eta_p{}^{\frac{1}{3}} \left(1 - \frac{7}{12} n^2\pi^2 \eta_p{}^{-\frac{2}{3}} \right), \tag{8d}$$

$$\omega_c^{(n)} \sim -\frac{\sqrt{2}}{P} \eta_p{}^{\frac{2}{3}} \left(1 - \frac{5}{12} n^2\pi^2 \eta_p{}^{-\frac{2}{3}} \right), \tag{8e}$$

$$R_c^{(n)} \sim \eta_p{}^{\frac{4}{3}} \left(3 + n^2\pi^2 \eta_p{}^{-\frac{2}{3}} \right), \tag{8f}$$

According to (8d,e,f), the modes of all n ($\ll \eta_p^{1/3}$) have the same critical Rayleigh numbers, wave numbers and phase velocities; i.e. they are excited to convection with equal ease. At that level approximation, it is not obvious that a "pure mode" such as (5) is "preferred" over a "mixed mode", i.e. one in which a combination of pure modes, having the same $\alpha = \alpha_c$ but involving several different values of n, are simultaneously excited (see below). Although this ambiguity is apparently settled at the more accurate level of approximation given by (8d)-(8e), which imply that pure modes are easier to excite to convection than mixed modes, marginal stability is not the only issue. In view of the ease with which other modes are excited, it is far from obvious that, once R exceeds R_c, a pure mode will be the preferred mode of convection.

To examine this question, (Lin *et al*, 1988) studied for both pure and mixed modes the finite amplitude convection that occurs for $R > R_c$. They developed an amplitude expansion, essentially in powers of $R/R_c - 1$ but more conveniently in powers of an amplitude parameter A, in which

$$\psi = A\psi_0 + A^2\psi_1 + A^3\psi_2, \tag{9a}$$

$$\theta = A\theta_0 + A^2\theta_1 + A^3\theta_2, \tag{9b}$$

$$R = R_0 + AR_1 + A^2R_2, \tag{9c}$$

and similarly for other variables such as ω and α. The expansions (9) were truncated at the level shown, using a solvability condition. The same level of amplitude truncation is employed in this paper. We shall use the term "truncation level"in a different sense below. Every term in expansion (9) is a product of a trigonometrical function of y and, for some n, a term of the form $\sin n\pi(x + \frac{1}{2})$. When we say in §3 that "the truncation level is N_T" we shall mean that N_T is the largest value of n appearing in $A\psi_0 + A^2\psi_1$. (ψ_2 and θ_2 are not fully determined; their role is confined to the consistency condition.) When ψ_0 is a linear combination of terms that involve $\sin n\pi(x + \frac{1}{2})$ for M different values of n, we shall say that we are dealing with an "M-mode"solution. Thus, a pure mode (5) corresponds to $M = 1$ but, as we increase A, we may need more terms to represent this solution. If [taking $n = 1$ in (5)] we add to (5) a term proportional to $\sin 2\pi(x + \frac{1}{2})$, we would describe the resulting solution as a "two-mode solution".

It would be pointless to write the real part of ψ_0, given by (5) with $n = 1$, as

$$\psi_0 = \left\{\hat{A}(t)\cos\alpha(y - ct) + \check{A}(t)\sin\alpha(y - ct)\right\}\sin\pi\left(x + \frac{1}{2}\right),$$

since, by a change of y origin, we could convert it to the simpler form

$$\psi_0 = \hat{A}(t)\cos\alpha(y - ct)\sin\pi\left(x + \frac{1}{2}\right).$$

But when we consider the $M = 2$ combination

$$\begin{aligned}\psi_0 = &\left\{\hat{A}(t)\cos\alpha(y - ct) + \check{A}(t)\sin\alpha(y - ct)\right\}\sin\pi\left(x + \frac{1}{2}\right)\\ &+ \left\{\hat{B}(t)\cos\alpha(y - ct) + \check{B}(t)\sin\alpha(y - ct)\right\}\sin 2\pi\left(x + \frac{1}{2}\right),\end{aligned} \tag{10}$$

it is not in general possible to eliminate both the $\check{A}$ and the $\hat{B}$ terms that would characterize the next approximation to a pure mode. Such mixed modes were one of the main concerns of Lin *et al* (1988).

We regard (10) as the crudest possible representation of a mixed mode, one that should however represent the solution well for the weakly nonlinear case in which A is small. As R is increased, more terms have to be added to (10) involving successively $\sin 3\pi(x + \frac{1}{2})$, $\sin 4\pi(x + \frac{1}{2})$, etc, corresponding to $M = 3$, $M = 4$, and so forth. If all the terms generated by the iteration are included in ψ_1, the truncation level increases rapidly. For this reason, Or and Busse (1987), in their Galerkin method, limited themselves to a base consisting of products of functions of x and y, there being M of the former and N of the latter, retaining only products for which $N + M \leq 6$. By repeating their calculation by their method (Or, 1985), we determined which of their terms had large amplitudes in their solutions and which had small. We verified that our expansion for $N_T = 6$ contained all of their large amplitude terms (and also others that they did not include).

Using (10) and its extensions to larger M, Lin *et al* (1988) were able to study in depth the period-doubling sequence, and transition to chaos, that the solution undergoes as R increased. To study double columns and their stability, two steps must be taken. First, double column arrays must be constructed and this can only be done by generalizing slightly what is meant by a "mixed mode". A double column structure can be formed from two pure modes of different n *but also of different* α:

$$\psi_0 = \left\{\hat{A}_1(t)\cos\alpha_1(y - ct) + \check{A}_1(t)\sin\alpha_1(y - ct)\right\}\sin\pi\left(x + \frac{1}{2}\right)$$
$$+ \left\{\hat{A}_2(t)\cos\alpha_2(y - ct) + \check{A}_2(t)\sin\alpha_2(y - ct)\right\}\sin 2\pi\left(x + \frac{1}{2}\right), \qquad (11)$$

where $\alpha_2 \neq \alpha_1$, so that one or other mode (or both) is not marginal in the sense of linear stability theory. Nevertheless, it is natural to take $\alpha_1 = \alpha_c$, as for the marginal mode, and to take α_2 close to the marginal value (8a), e.g. $\alpha_2 = 1{\cdot}1\,\alpha_c$. We found by numerical experimentation that, if we fixed $\alpha_1 = \alpha_c$, the double structure (11) of permanent form existed for all R in excess of a threshold value that depended on α_2/α_1. That threshold was, for values of α_2/α_1 close to unity, only a few percent greater than R_c for the pure mode (5). For small supercritical values of R, we found that we could reproduce the results of Or and Busse (1987) to better than 0.3% accuracy by taking $M = 2$. As for the case (10), when R is increased towards the onset of chaos, it is necessary to increase M beyond 2 in order to obtain what we may call "limiting behavior", i.e. solutions that are insensitive to a further increase in M, and therefore appear to be convincingly converged. For these large values of R and for $P = 1$, we generally took $M = 8$, corresponding to a truncation level N_T of 16, and could then reproduce the results of Or and Busse to about 0.5% accuracy. For large R but smaller values of the Prandtl number ($P = 0.7$), we needed fewer modes. In order to make these comparisons it was necessary to repeat, and to take into new parameter regimes, the Galerkin calculations of Or and Busse.

It is clear from the structure of equations (3) that, in a finite amplitude solution initiated from (11), the mode of wavenumber

$$\alpha_3 = |\alpha_1 - \alpha_2|$$

will figure in ψ_1 and θ_1, etc. Also, starting from (11), the nonlinear interactions in (3) introduce terms proportional to $\sin\pi\,(x+\frac{1}{2})$ and $\sin 3\pi\,(x+\frac{1}{2})$] They do not, however, produce what is needed in order to create double column instability, namely a y-independent part to ψ_1, corresponding to a mean flow, $\mathbf{V}(x,t)$, down the channel:

$$\mathbf{V} \;=\; V\,\hat{\mathbf{y}} \;=\; -\,\Psi_x(x,t)\,\hat{\mathbf{y}}, \tag{12}$$

where

$$\Psi(x,t) \;=\; \langle\,\psi(x,y,t)\rangle, \tag{13}$$

the angle brackets denoting the y-average of the quantity between them. Or and Busse (1987) found a mean flow by iterating the double column structure (11) to the third order in A, but the mean flow they obtained was not sufficiently large to create marked banding in the convection pattern.

It follows from (3a) that the mean flow is governed by

$$\partial_t V \;=\; \langle M\rangle \;+\; \partial_x^2 V, \tag{14}$$

where

$$M \;=\; (\partial_y\psi'\partial_x \;-\; \partial_x\psi'\partial_y)\,\partial_x\psi', \tag{15}$$

and ψ' denotes the averageless part of ψ:

$$\psi' \;=\; \psi \;-\; \Psi. \tag{16}$$

The quantity M represents the mean momentum flux created by the convection, and $\partial_x^2 V$ the destruction of mean momentum by viscosity. Though (14) lacks a buoyancy source, the absence of a y-derivative in the diffusion term suggest that $\langle M\rangle$ will produce a larger effect on V than M' will on ψ', since diffusion more effectively reduces ψ' by the large factor $1 \;+\; (\alpha/\pi)^2 \gg 1$; see (9a) and recall that $\eta_p \gg 1$.

The second step of the program is now clear: one should seek solutions in which the α_3 mode has greater amplitude by initiating the expansion (9) using

$$\begin{aligned}
\psi_0 \;=\; &\left\{\hat{A}_1(t)\cos\alpha_1(y-ct) \;+\; \check{A}_1(t)\sin\alpha_1(y-ct)\right\}\,\sin\pi\left(x+\frac{1}{2}\right)\\
&+\;\left\{\hat{A}_2(t)\cos\alpha_2(y-ct) \;+\; \check{A}_2(t)\sin\alpha_2(y-ct)\right\}\,\sin 2\pi\left(x+\frac{1}{2}\right)\\
&+\;\left\{\hat{A}_3(t)\cos\alpha_3(y-ct) \;+\; \check{A}_3(t)\sin\alpha_3(y-ct)\right\}\,\sin 3\pi\left(x+\frac{1}{2}\right).
\end{aligned} \tag{17}$$

This starting point is only one of many: one could, for instance, generate a similar solution in which the $\sin 3\pi\,(x+\frac{1}{2})$ of the last term in (17) is replaced by $\sin\pi\,(x+\frac{1}{2})$, this term being also resonant with the other two, according to (3). We decided to pursue (17) simply because the resulting flow structures seemed to fit well to Busse's concept of double-column instability.

When we iterate starting from the resonant triad (17), we obtain ψ_1 containing a very large number of terms, namely $\sin 2\pi(x + \frac{1}{2})$, $\sin 4\pi(x + \frac{1}{2})$, $\sin 6\pi(x + \frac{1}{2})$, $\sin \pi(x + \frac{1}{2})\cos[\alpha_3 (y - ct)]$, $\sin \pi(x + \frac{1}{2})\sin[\alpha_3 (y - ct)]$, $\sin \pi(x + \frac{1}{2})\cos[(\alpha_2 + \alpha_3)(y - ct)]$, $\sin \pi(x + \frac{1}{2})\sin[(\alpha_2 + \alpha_3)(y - ct)]$, $\sin 2\pi(x + \frac{1}{2})\cos[(\alpha_1 - \alpha_3)(y - ct)]$, $\sin 2\pi(x + \frac{1}{2})\sin[(\alpha_1 - \alpha_3)(y - ct)]$, $\sin \pi(x + \frac{1}{2})\cos[(\alpha_1 + \alpha_2)(y - ct)]$, $\sin \pi(x + \frac{1}{2})\sin[(\alpha_1 + \alpha_2)(y - ct)]$, $\sin 5\pi(x + \frac{1}{2})\cos[(\alpha_2 + \alpha_3)(y - ct)]$, $\sin 5\pi(x + \frac{1}{2})\sin[(\alpha_2 + \alpha_3)(y - ct)]$, $\sin 4\pi(x + \frac{1}{2})\cos[\alpha_2 (y - ct)]$, $\sin 4\pi(x + \frac{1}{2})\sin[\alpha_2 (y - ct)]$, $\sin 4\pi(x + \frac{1}{2})\cos[(\alpha_1 - \alpha_3)(y - ct)]$, $\sin 4\pi(x + \frac{1}{2})\sin[(\alpha_1 - \alpha_3)(y - ct)]$, $\sin 3\pi(x + \frac{1}{2})\cos[(\alpha_1 + \alpha_2)(y - ct)]$, $\sin 3\pi(x + \frac{1}{2})\sin[(\alpha_1 + \alpha_2)(y - ct)]$, $\sin 5\pi(x + \frac{1}{2})\cos[\alpha_1(y - ct)]$, $\sin 5\pi(x + \frac{1}{2})\sin[\alpha_1(y - ct)]$, as well as additional contributions to the six resonant terms shown in (17). The consistency condition could, in fact, be applied here, but instead we sought results to higher accuracy by absorbing these terms into ψ_0 and closing the expansion at the ψ_2 level by applying a consistency condition in the usual way.

It may be seen that the first three of the terms just listed are parts of a mean flow, V. It may also be seen, from the large number of terms arising in this $M = 3$, $N_T = 6$ case, all of which were retained in the calculations that will be described below, why the task of computing the coefficients is most expeditiously and reliably left to a symbolic manipulation program (MACSYMA).

In the next section we show the results of applying this program of research, but we should note finally one very significant point. Double-column instability is a finite amplitude instability. When we generate a solution using (11) and perturb it infinitesimally, we find that the eigenvalues, i.e. the growth rates, all have negative real parts: the double-column structure is linearly stable. Nevertheless, provided the Rayleigh number, R, is in the right range, two distinct solutions exist, given to leading order by (11) and (17) respectively, the latter having the more vigorous motions. This indicates that, when the structure (11) is subjected to a sufficiently large perturbation, it will make a transition to (17), i.e. double-column instability is a finite amplitude phenomenon.

3. Results

Lin *el al* (1988) discovered that there are two distinct types of solutions (10) of permanent form, i.e. solutions that, though translating in the y-direction, are stationary in that moving frame. They called these "Solution I" and "Solution II". The phase difference between the α_1 and α_2 components is large in Solution I (approximately $\pm 2\pi/3$), but is small in Solution II (approximately $\pm\pi/12$); this phase difference is the characteristic by which the two solutions can be distinguished. A similar situation arises when the two components of ψ_0 have different y wavenumbers, as in (11). In Figs.4 we show, for both Type I solutions and Type II solutions, the streamfunctions of the double column structures that arise when we develop solutions to (3) starting from (11); in each case, $\alpha_1 = \alpha_c$, $\alpha_2 = 1.1\alpha_c$ and $B = 38000$. Here $B = R/P$ is the so-called "buoyancy parameter", an alternative to the Rayleigh number R that we shall use in this section (we shall throughout assume that $P = 0.7$).

Each of Figs.4 shows, at any fixed x (corresponding to a fixed radial distance in the planetary application), an alternation of easterly and westerly jets as y changes (corresponding to varying planetary longitude). The figures also show two columns of vortices that would

correspond on a planet like Jupiter to two bands. By including more modes, it might be possible to mimic the five bands seen in Jupiter's atmosphere, but there is a more serious difficulty. Evidently the alternation of zonal motion within each band of Figs.4 does not correspond to the unidirectional flow seen in each planetary band. To obtain bands of alternating zonal flow, we vizualise that the double column structures shown in Figs.4 are subject to a finite amplitude instability that carries them to states in which the modes α_1, α_2 and $\alpha_3 = |\alpha_1 - \alpha_2|$ strongly resonate. The result of such an instability will be a flow that can be obtained by solving (3) subject to starting conditions (17).

We have noted in §3 that the double column structures (11) exist stably only when R exceeds a certain threshhold value, dependent on α_2/α_1. The situation is similar for the resonating wave structures (17) associated with double column instability. Fig. 5 shows a plot of $(B - B_c)/B_c$ as a function of wavenumber α. The wave number α is normalized by dividing by α_c, the critical wavenumber at which B takes the minimum value, B_c, at which convection can marginally occur as a pure mode. The marginal curve for the $n = 1$ modes at other wavenumbers is shown in Fig. 4, and lying above it (but not intersecting it) is the corresponding marginal curve for $n = 2$; see (6b). The third curve is for $n = 3$. The double column structures, obtained by solving (3) starting from (11), exist above the lower of the two dashed curves shown on the right-hand ($\alpha > 1$) side of the figure.

Of greatest interest in Fig.5 are the shaded regions, which result from integrations of (3) starting from (17). The boundaries of the shaded regions give threshold values of B as functions of α_2/α_c (right-hand curve) and α_3/α_c (left-hand curve). Within these shaded regions a solution (17) of permanent form can exist. There is a correspondence between the left-hand and right-hand areas: a point in one area is related to only one point in the other area, namely the point that completes the resonant triad for that particular value of B.

To obtain the boundaries delineated in Figs.5 by dashed curves, a linear stability problem was solved by two distinct methods. The first of these was a Fourier expansion method. We combined each pair of A coefficients in (11) or (17) into one complex amplitude, $\bar{A}$ say, and wrote for every such $\bar{A}$,

$$\bar{A} = \sum_{j=-J}^{J} \bar{A}_j \, e^{ij\omega t}. \tag{18}$$

We then searched for the values of B for which ω is real. Limitations of computer resources compelled us to truncate the sums (18) after 17 terms ($J = 8$). The second, and less accurate, method was Runge-Kutta integration. This forward integration in time determines, after an initial period in which transient, highly damped modes disappear, whether the solution grows or disappears for the B that was selected. That value of B was adjusted until a solution was obtained that preserved its amplitude during the time of integration.

The agreement between the results of these two methods of determining the marginal states was satisfactory for $\alpha_3 = 0.1\alpha_c$, but deteriorated as α_3 was reduced. Although Fig.5 incorporates results for α_3 as small as $0.01\alpha_c$, we do not believe that they are completely trustworthy for $\alpha_3 < 0.04\alpha_c$, which seems to be close to the minimum of the left-hand dashed curve in Fig.5. To obtain more reliable results, we believe that the truncation level

in (18) should be raised above $J = 8$. As α_3 was increased beyond $0.25\alpha_c$, the marginal B grew very rapidly, and we cannot rule out the possibility that the dashed curve possesses an asymptote. Again the numerical method began to perform too poorly for us to determine whether this was the case.

An objection might be raised at this point. It seems little short of miraculous that a mode having such a small wavenumber as $0.1\alpha_c$ for α_3, which for these values of R is so strongly subcritical on linear theory (i.e.lies so far beneath the $n = 3$ curve in Fig.5), could contribute in any way to the resonance. Surely the α_3 mode must merely be a slave driven into motion by the interaction of the α_1 and α_2 modes and must strongly extract energy from them? It seems to us that such a view would be a little simplistic. It should be recalled that, because of its very long y-wavelength, the viscous dissipation rate per unit horizontal (yz) area of the α_3 mode is very small compared with those of the α_1 and α_2 modes. It is therefore easily driven into motion. It is strongly subcritical on linear theory only because, slight as its energy demands are, the rising and sinking convection currents (widely separated on the $2\pi D/\alpha^3$ lengthscale) are unable to inject power at a sufficient rate to sustain the mode. The nonlinear interaction of the α_1 and α_2 modes can therefore excite the α_3 mode to large amplitude with little cost to themselves. As α_3 and α_2 are increased towards $0.3\alpha_1$ and $1.3\alpha_1$ however, they begin to make greater energy demands, and the right-hand sides of the boundaries of the shaded areas in Fig. 5 therefore move towards larger values of R.

With the computer resources available to us, we were not able to undertake a detailed study of resonances for which $\alpha_2 < \alpha_1$, but the limited exploration we made suggested that there exists a similar shaded area just to the left of $\alpha/\alpha_c = 1$, and a corresponding area of resonant states at small α_3/α_1, where now $\alpha_3 = \alpha_1 - \alpha_2$. Perhaps these areas also possess a minimum B, but if so our preliminary results would indicate that it exceed the mimimum B shown for the $\alpha_2 > \alpha_1$ states in Fig. 5. Another possibility is that there is a single continuous curve defining double column solutions, in which α_2 extends both to the right and to the left of α_1. Similarly the shaded area of resonant solutions would cross $\alpha_2 = \alpha_1$ smoothly, the minimum of the entire curve being, as shown in Fig. 5, to the right of $\alpha_2 = \alpha_1$. In this context, the possible loss of numerical accuracy near $\alpha_2 = \alpha_1$ (see above) should not be forgotten, and the apparent increase of the marginal B near $\alpha_2 = \alpha_1$ should not be given too much weight.

Streamfunctions for Solutions I and II, obtained from (17), are shown in Figs.6, again for $\alpha_1 = \alpha_c$, $\alpha_2 = 1.1\alpha_c$ and $B = 38000$. Solution II displays clearly a central band of almost unidirectional flow, on each side of which lie bands in which the y-motion is directed in the opposite sense to the central band, and which contain vortices all of the same sense of circulation. The alternation in mean motion, V, is displayed in Figs.7. It is suggested that this would correspond in a major planet to easterly and westerly wind layering. It may also be noticed that the characteristic velocities corresponding to solutions (17) are significantly greater than for solutions (11), suggesting that the motions shown in Figs. 6 are "preferred" to the double column structures shown in Figs. 4.

It is interesting to observe the change in structure of the resonating modes as α_3 is increased. When (in place of $\alpha_1 = \alpha_c$, $\alpha_2 = 1.1\alpha_c$, and $\alpha_3 = 0.1\alpha_c$) we started from $\alpha_1 = \alpha_c$, $\alpha_2 = 1.2\alpha_c$, and $\alpha_3 = 0.2\alpha_c$ for $B = 40000$, and again sought strongly

resonating solutions by solving (3) subject to (17), we obtained the flows shown in Figs.8. The continuity of the zonal flow in clearly severely broken. This trend persisted when we took $\alpha_1 = \alpha_c$, $\alpha_2 = 1.3\alpha_c$, and $\alpha_3 = 0.3\alpha_c$. In this case, no very obvious layering could be discerned. We conclude that layering depends crucially on the presence of two large, almost equal, wavenumbers and one small wavenumber, their difference.

It is perhaps a little remarkable that the behavior of the multi-α solutions as B is increased parallels in most respects the behavior of the mixed mode solutions of one wavenumber [see (10)] studied by Lin *et al* (1988). Tables I and II show the locations of the critical and higher bifurcation points of the double column instability for Solution I and II respectively. The first set of rows in each table give data for the double column solution, the second gives that for the first resonance case considered above ($\alpha_3 = 0.1\alpha_c$), and the final set of rows give the same information for the second resonance case ($\alpha_3 = 0.2\alpha_c$). The first two columns define the case, and the truncation level to which the solutions were taken. The next column records the value of B for criticality ($B = B_s$), and the next column locates the first, period-doubling bifurcation ($B = B_d$). The subsequent columns give the values of B at which the period quadruples (B_q), is increased eightfold (B_8), and becomes sixteen times as large (B_{16}). Subsequently, the solution becomes aperiodic (B_a). Table II has an extra column giving B_{qu} marking the onset of a quasi-periodic regime preceding the aperiodic solutions.

A different property of the same solutions is recorded in Tables III. Here is plotted

$$Q_n = \frac{R_{n+1} - R_n}{R_{n+2} - R_{n+1}} \tag{19}$$

for the successive bifurcations. According to Feigenbaum (1977, 1984), this should, as n increases, tend to 4.67 in all cases, and Tables III confirm this satisfactorily. Such tests of Universality were central to the paper of Lin *et al* (1988) and will not be labored here.

4. Conclusions

The barotropic annulus provides perhaps the clearest possible demonstration of thermal Rossby waves, as the convection in a rotating system with sloping end walls is usually called. In their simplest form, these waves consist of drifting columns with their axes parallel to the rotation axis, and alternately of one sign of vorticity along that axis (as measured in the frame co-rotating with the system) and then of the other. Such convection patterns may arise in Nature, in the equatorial regions of the thick atmospheres of the major planets, Jupiter and Saturn. The convective columns, one imagines, would cross from one hemisphere of the atmosphere to the other, and would (where they meet the top of the planetary atmosphere) form a sequence of latitudinal bands round each of which the columnar vortices would be strung, as in a necklace. Indeed, such bands are seen on the faces of the major planets but, if we attempt to relate the convection model to the planets, we encounter a significant difficulty: the bands observed on the planets are associated with a strong zonal wind structure. This flow is, as a function of latitude, alternately to the East and to the West. To be tenable as a model of the planets, we must understand how columnar convection can generate such a mean flow. This has been the central issue of this paper, and we have discovered what we believe to be a viable mechanism.

We have focussed on two latitude bands, which we have been able to simulate by studying a compound thermal Rossby wave consisting of two nearly equal zonal wavenumbers, where by 'zonal'in the straight geometry of the annulus we mean 'along the axis'of the annulus. The resulting flow structure consists of two rows of vortex cells, which we have called a 'double column'solution. Little mean flow is associated with this convection pattern; it is stable on linear theory. We have found, however, that a related structure exists which consists of these two thermal Rossby waves plus a third thermal Rossby wave that completes a resonant triad of zonal wavenumbers. We have supposed that this flow regime could be brought about by a finite amplitude perturbation of the double column structure, and we have therefore described it as 'double column instability'.

The characteristic difference between a double column structure and the state resulting from its double column instability is profound. The vorticity distribution of the double column solution is completely redistributed by the instability, the columns of one sense of vorticity congregating in one latitude band, those of the opposite vorticity collecting in the other. It is clear from an elementary consideration of the change in circulation resulting from this redistribution of vorticity that a large mean flow develops, so providing what seems to us to be at least the germ of an explanation for the rapid variation of zonal wind with latitude observed in the major planets.

Aknowledgements.

During the initial phases of this work, I was a member of the Department of Atmospheric Sciences, and was supported by grant (443956-23320), awarded to Professor Michael Ghil by NASA. I want to thank him and to Professor George Siscoe for their interest in this work. During its completion, I was supported by grant N00014086-K-0641 from the Office of Naval Research (Principal Investigator: Paul H. Roberts). I am extremely grateful to Professor Roberts for advising me on all aspects of this work, and for helping me to understand many of the physical mechanisms at work in my model. Without his help, this paper would not have been completed at this time.

References

Busse, F. H., "Thermal instabilities in rapidly rotating systems," **J. Fluid Mech., 44,** 441-460 (1970).

Busse, F. H., "A simple model of convection in the Jovian atmosphere," **Icarus 29,** 255-260 (1976).

Busse, F. H., "Non-linear properties of thermal convection," ***Repts. Progr. in Phys.**, 41, 1931-1967 (1978).*

Busse, F. H., "A model of mean zonal flows in the major planets," **Geophys. Astrophys. Fluid Dynam., 23,** 153-174 (1983).

Feigenbaum, M. J., "Quantitative universality for a class of nonlinear transformations," **J. Stat. Phys., 19,** 25-52 (1977).

Feigenbaum, M. J., "Universal behavior in nonlinear systems", 49-84 in **Universality in Chaos.** (Ed. P. Cvitanovic), Adam Hilger, Bristol, England, (1984).

Hatzes, A., Wenkert, D. D., Ingersoll, A. P. and Danielson, G. E., "Oscillation and velocity structure of a long-lived cyclonic spot". J. **Geophys. Res., 86, A10,** 8745-8749 (1981).

Ingersoll, A. P. "Jupiter and Saturn", 60-70, in **The Planets**. (Ed. B. Murray), Scientific American, New York, San Francisco. (1981).

Lin, R.-Q., "A hierarchy of perturbative models for solving nonlinear problems in geophysical fluid dynamics: Systematic use of symbolic Manipulation", **Ph.D. thesis** (1988).

Lin, R.-Q., F. H. Busse, and M. Ghil, "Transition into two dimensional turbulent convection in a rapidly-rotating annulus," to appear in **Geophys. & Astrophys Fluid Dynam.** (1988).

Or, A. C., "Buoyancy-driven instabilities in a rapidly rotating cylindrical annulus", **Ph.D. thesis** (1985).

Or, A. C., and Busse, F. H., "Convection in a rotating cylindrical annulus. Part II: Transitions to asymmetric and vacillating flow", **J. Fluid Mech., 174,** 313-326 (1986).

Roberts, p. H., "On the thermal instability of a rotating-fluid sphere containing heat sources", **Philos. Trans. R. Soc. London A 263**, 93-117 (1968).

Williams, G. P., "Jupiter's atmospheric convections," ***Nature***, ***257***, 778 (1975).

Williams, G. P., "Planetary circulations: 1. Barotropic representation of Jovian and terrestrial turbulence," ***J. Atmos. Sci.***, ***35***, 1399-1426 (1978).

Williams, G. P., "Planetary circulations: 2. The Jovian quasi-geostrophic regime," **J. Atmos. Sci., 36**, 932-968 (1979a).

Williams, G. P., "Planetary circulations: 3. The terrestrial quasi-geostrophic regime," **J. Atmos. Sci., 36**, 1409-1435 (1979b).

Williams, G. P., "Jovian and comparative atmospheric modeling," in **Issues in Atmospheric and Ocean Modeling. Part A: Climate Dynamics,** (Ed. Syukuro Manabe), Academic press, **Advance in Geophysics. 28**, 381-429 (1985).

LEGENDS FOR FIGURES

1. (a) Photograph of banding in the atmosphere of Jupiter as seen by Voyager 1. (Courtesy of NASA.)

(b) Busse's (1983) conception of how such planetary banding arises. (Reproduced from *Geophysical and Astrophysical Fluid Mechanics*, with permission.)

2. Zonal velocity profiles from the north polar and south polar regions of Jupiter's atmosphere (Hatzes *et al*, 1981; reproduced from *Journal of Geophysical Research*, with permission).

3. The barotropic annulus.

4. Double column solutions. Streamfunctions are shown for one complete period for $B = 38000$, $\alpha_1 = \alpha_c$, $\alpha_2 = 1.1\alpha_c$, and $P = 0.7$. (a) Solution I, (b) Solution II.

5. The regions of parameter space in which double column structures and resonant structures exist, for $P = 0.7$. The x-axis is α/α_c, the y-axis is $(B - B_c)/B_c$, where α_c is the critical wavenumber on linear theory and B_c is the corresponding value of the buoyancy parameter B. For further explanation, see text.

6. The resonant structures. Streamfunctions are shown for one complete period for $B = 38000$, $\alpha_1 = \alpha_c$, $\alpha_2 = 1.1\alpha_c$, $\alpha_3 = 0.1\alpha_c$ and $P = 0.7$. (a) Solution I, (b) Solution II.

7. The mean flows corresponding to the solutions shown in Fig. 6. (a) Solution I, (b) Solution II.

8. The resonant structures. Streamfunctions are shown for one complete period for $B = 40000$, $\alpha_1 = \alpha_c$, $\alpha_2 = 1.2\alpha_c$, $\alpha_3 = 0.2\alpha_c$ and $P = 0.7$. (a) Solution I, (b) Solution II.

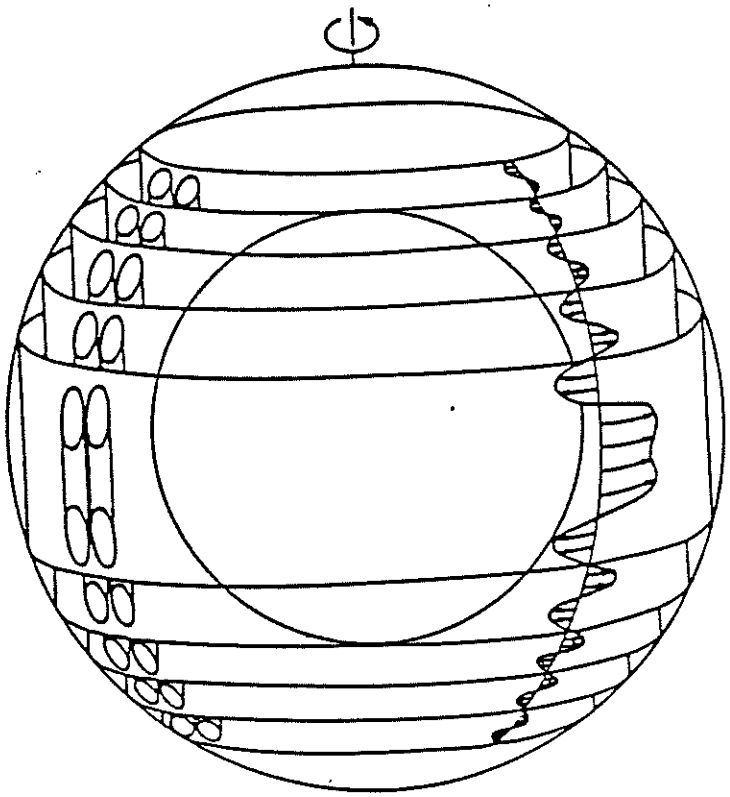

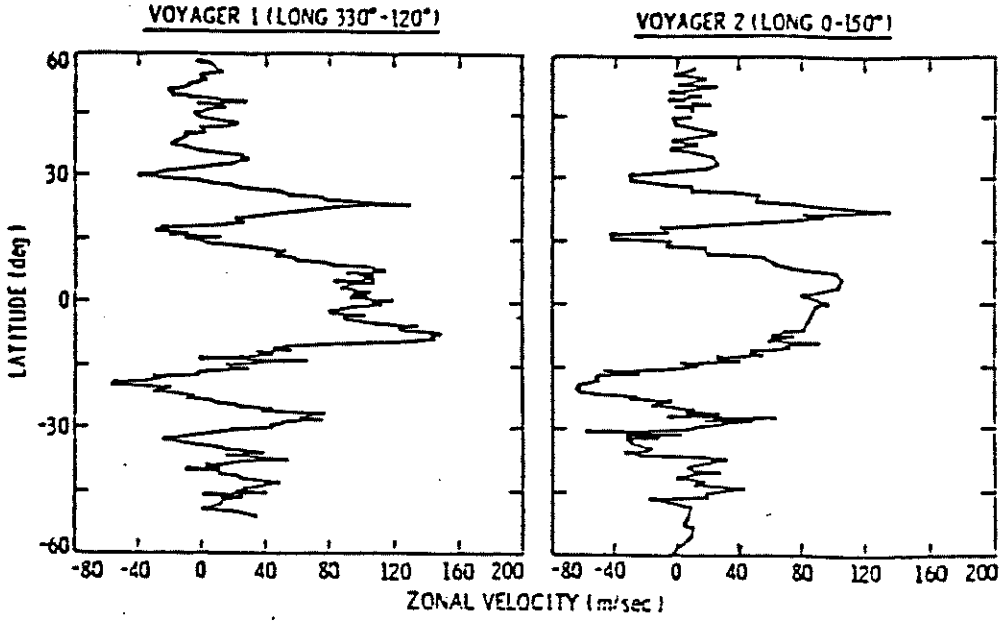
VOYAGER 1 (LONG 330°-120°)
VOYAGER 2 (LONG 0-150°)
60
30
0
-30
-60
LATITUDE (deg)
-80 -40 0 40 80 120 160 200
-80 -40 0 40 80 120 160 200
ZONAL VELOCITY (m/sec)

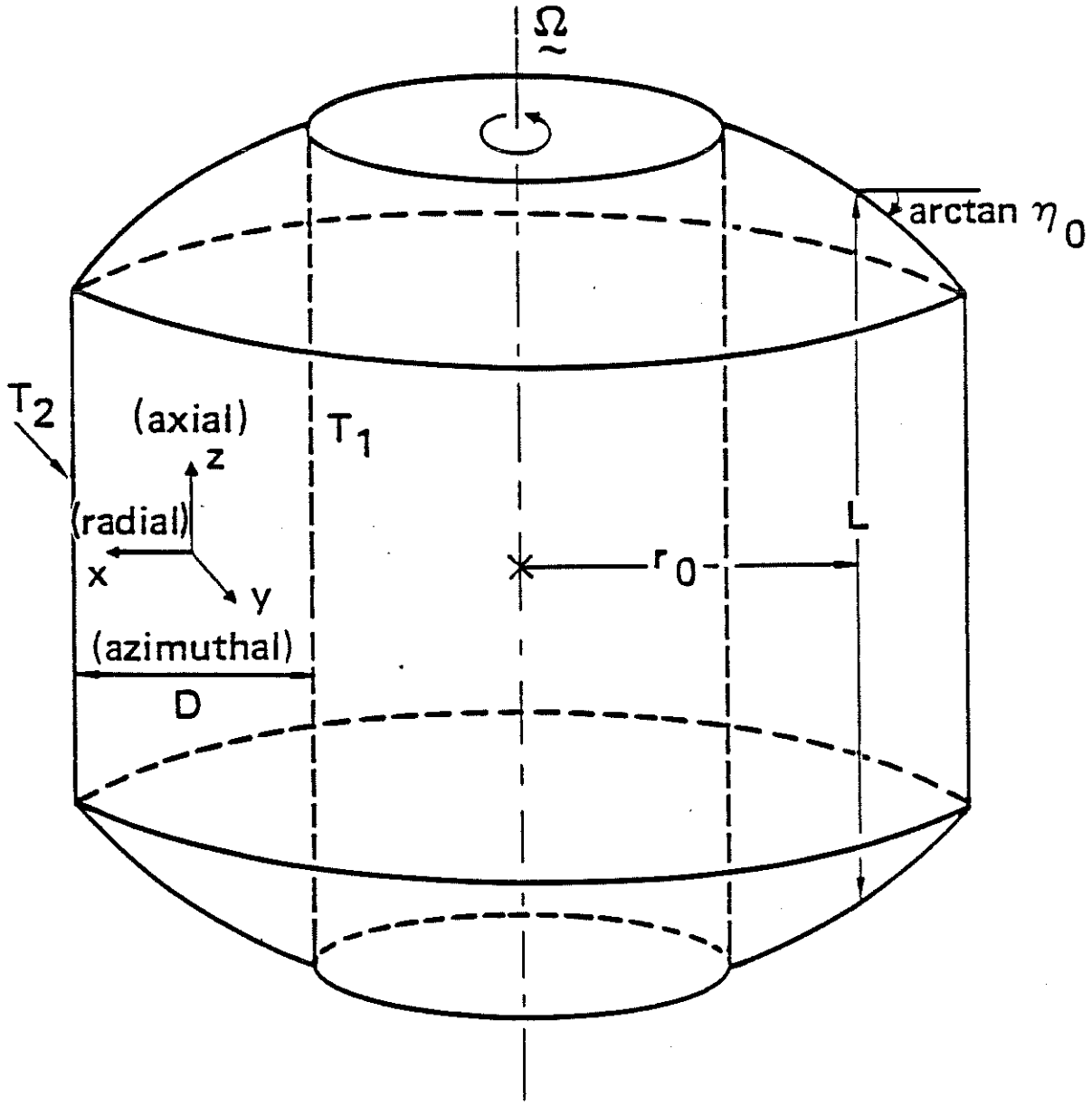
Ω
arctan η_0
T_2
(axial)
z
T_1
(radial)
x
y
L
r_0
(azimuthal)
D

Solution I

T = 0.0

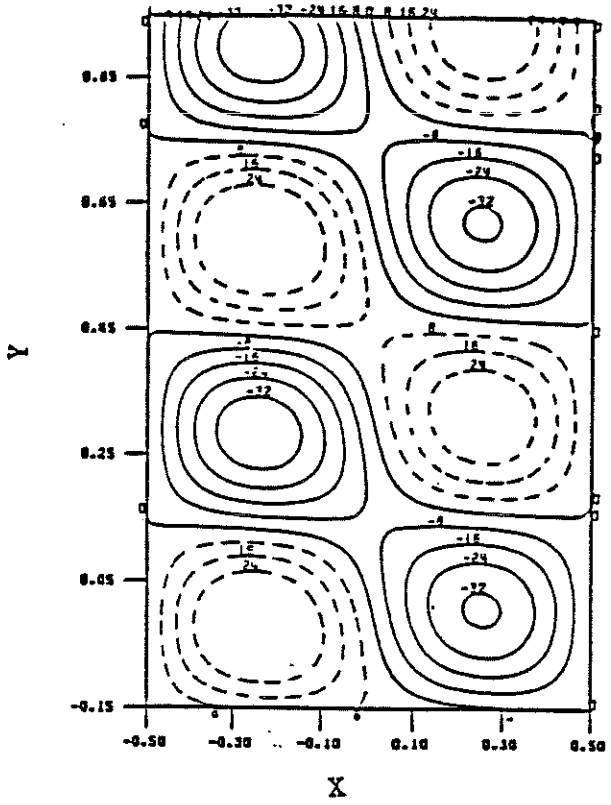

T = 0.08

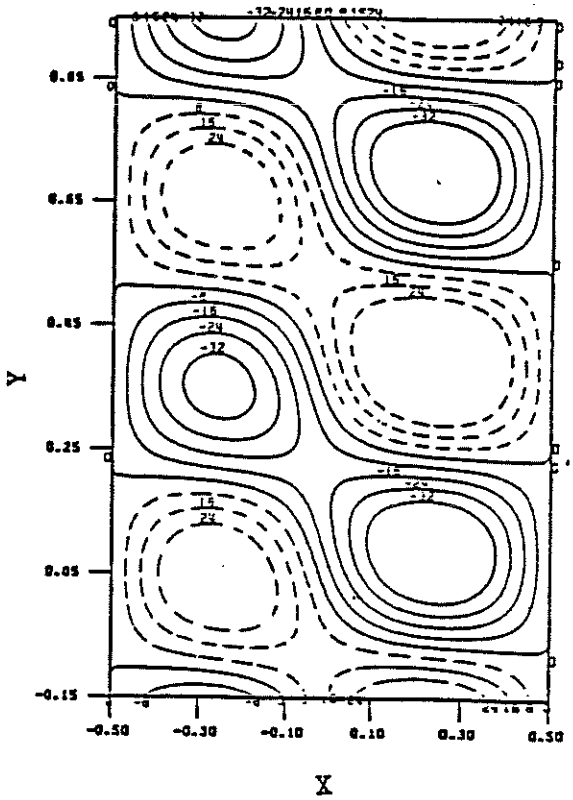

T = 0.17

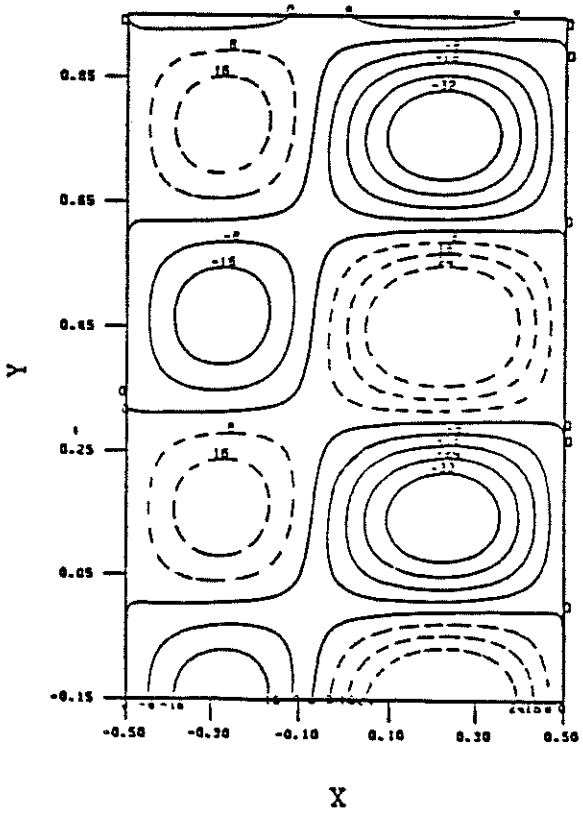

T = 0.26

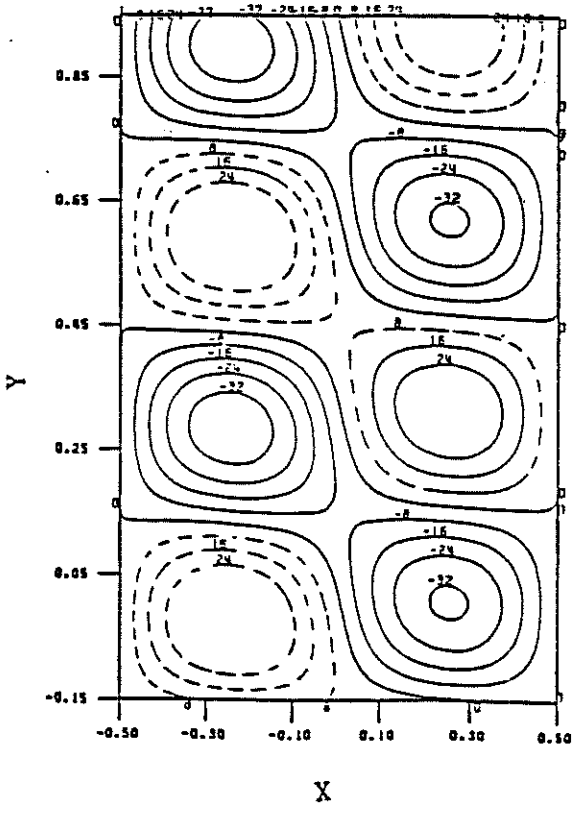

Solution II

T = 0.0

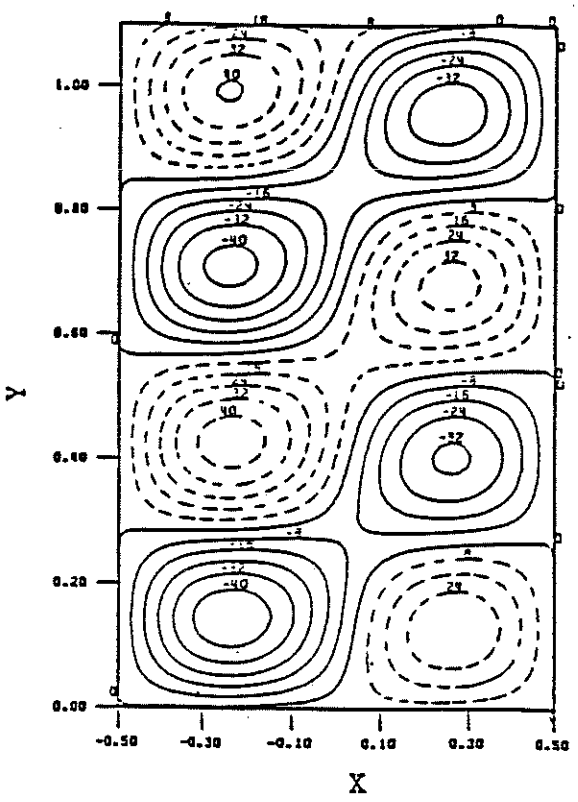

T = 0.14

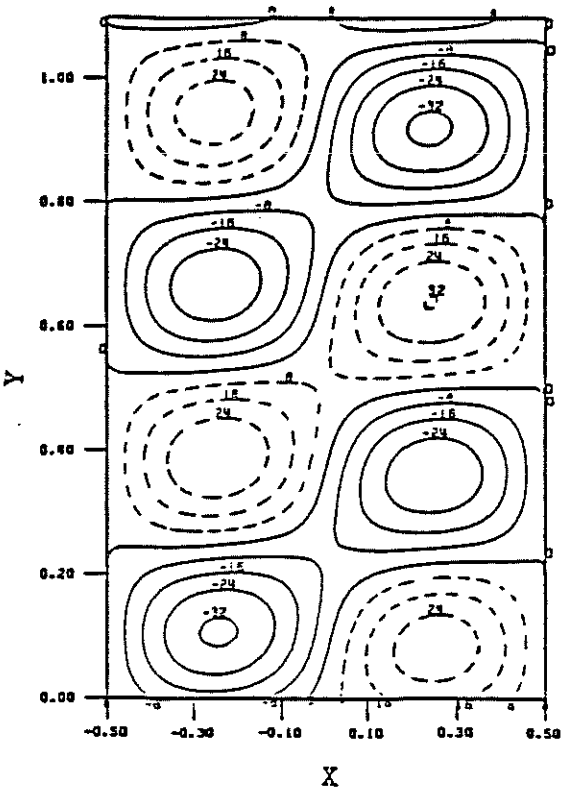

T = 0.29

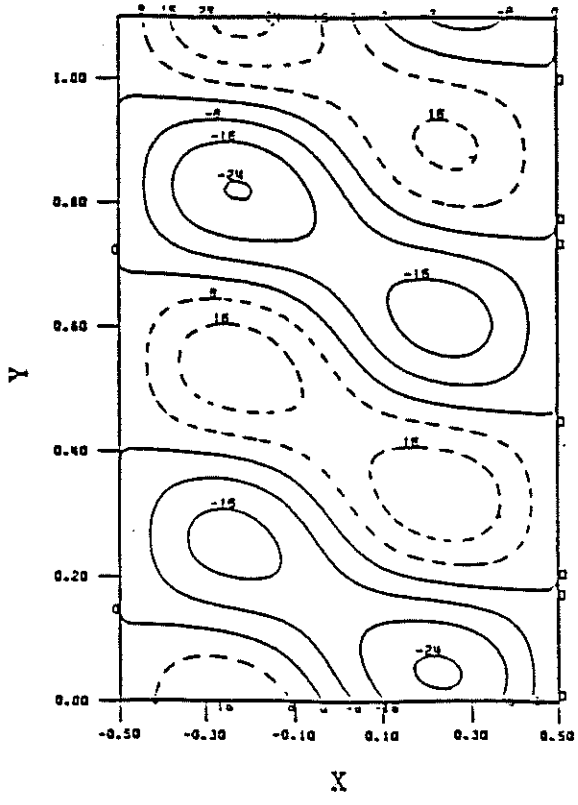

T = 0.44

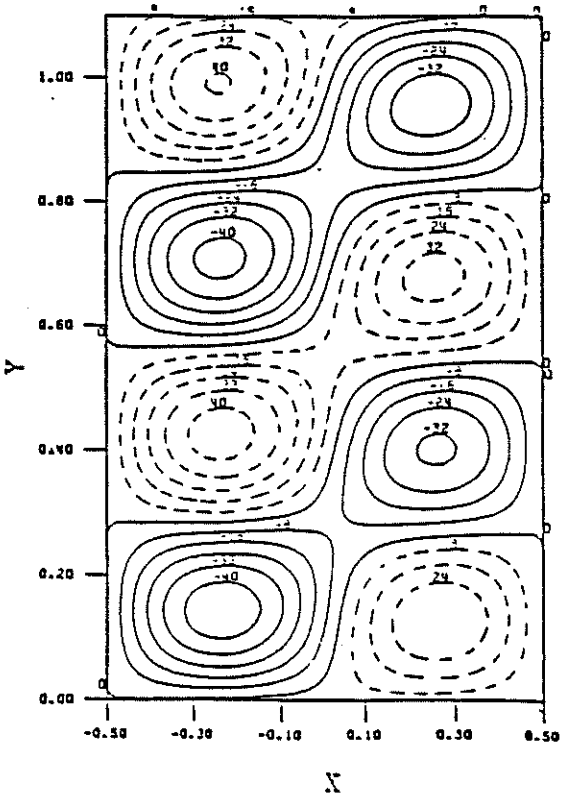

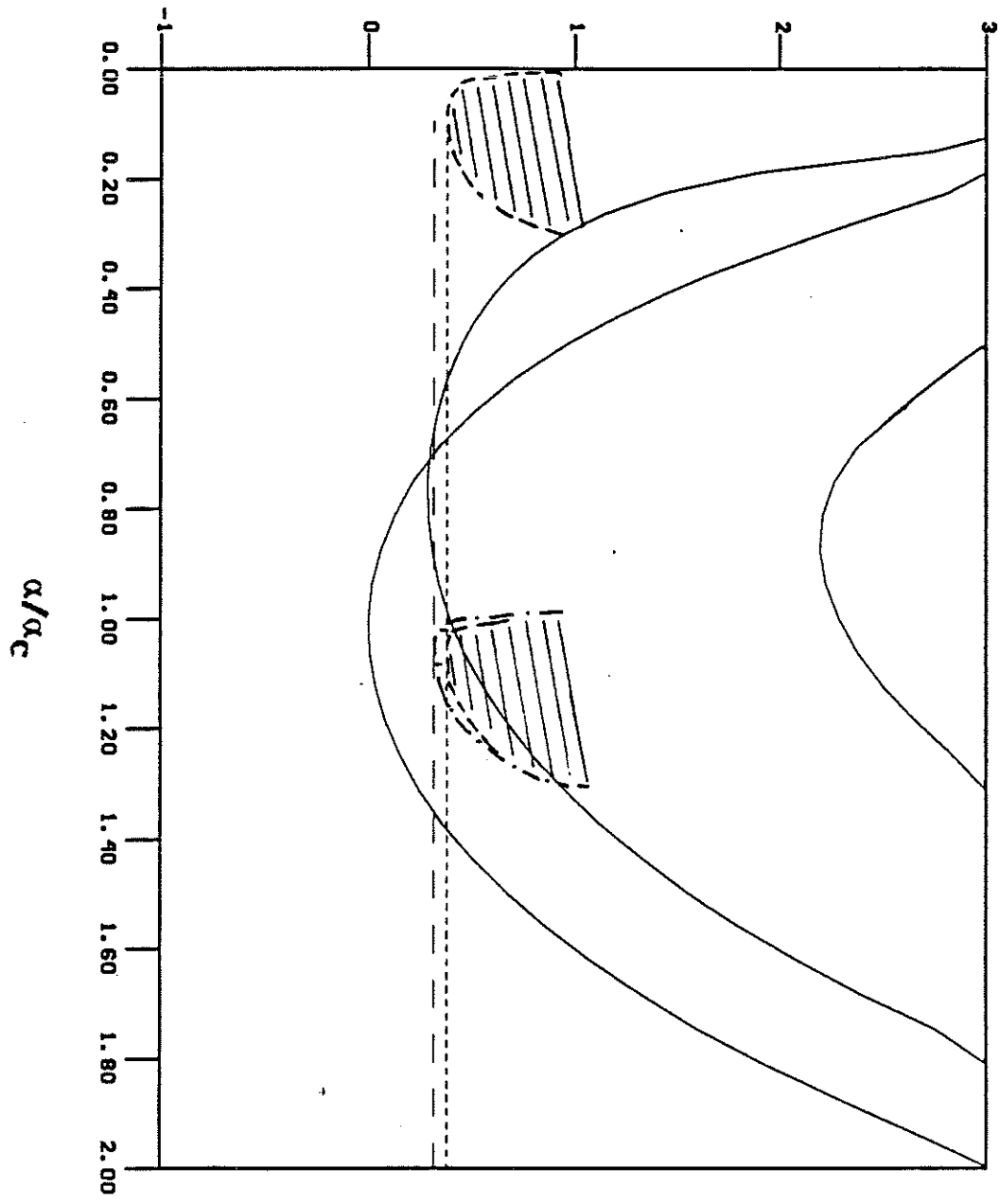
$(B - B_c)/B_c$
-1
0
1
2
3
0.00
0.20
0.40
0.60
0.80
1.00
1.20
1.40
1.60
1.80
2.00
α/α_c

Solution I

T = 0.0

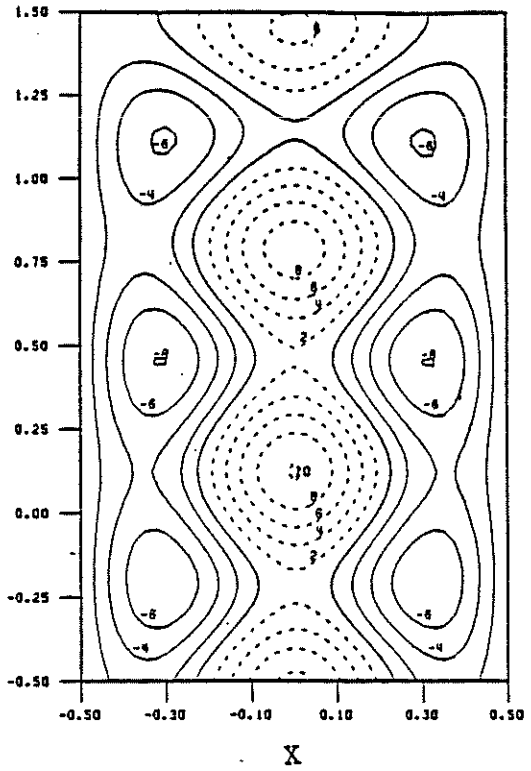

T = 0.12

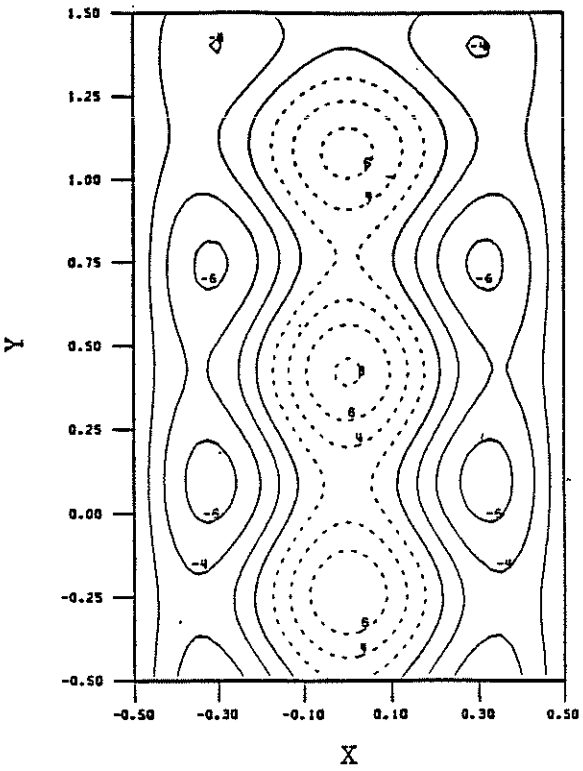

T = 0.24

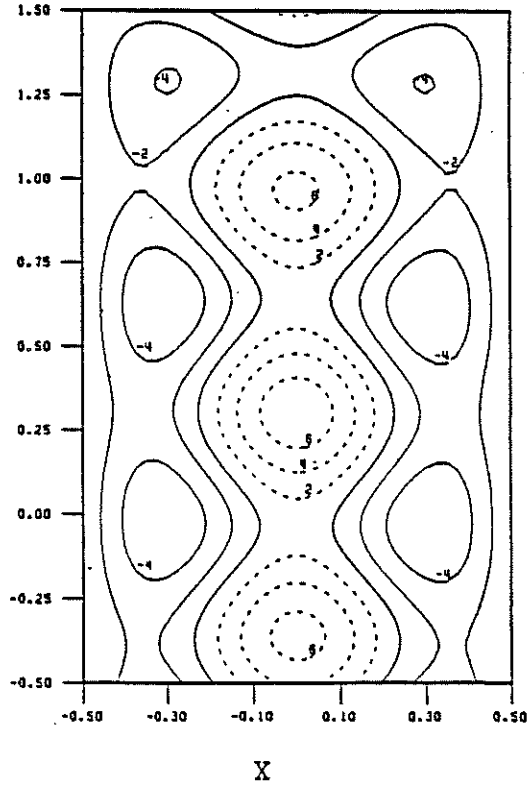

T = 0.36

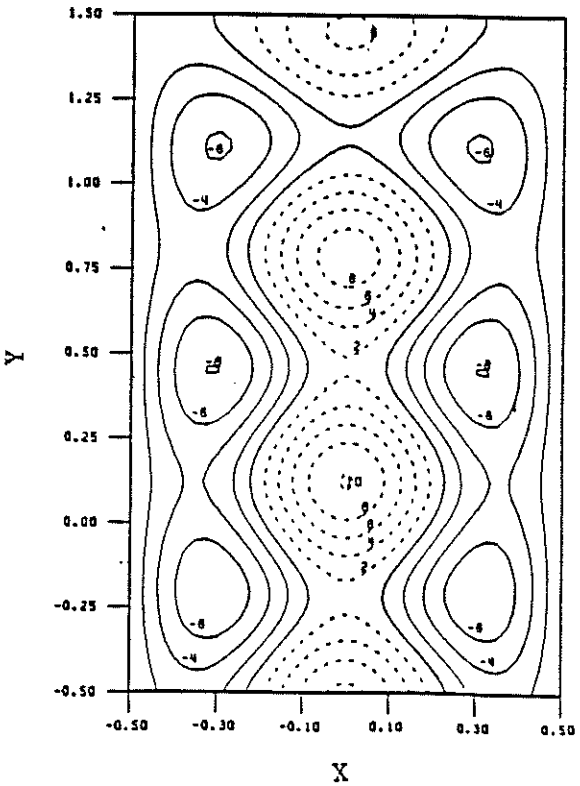

Solution II

T = 0.0

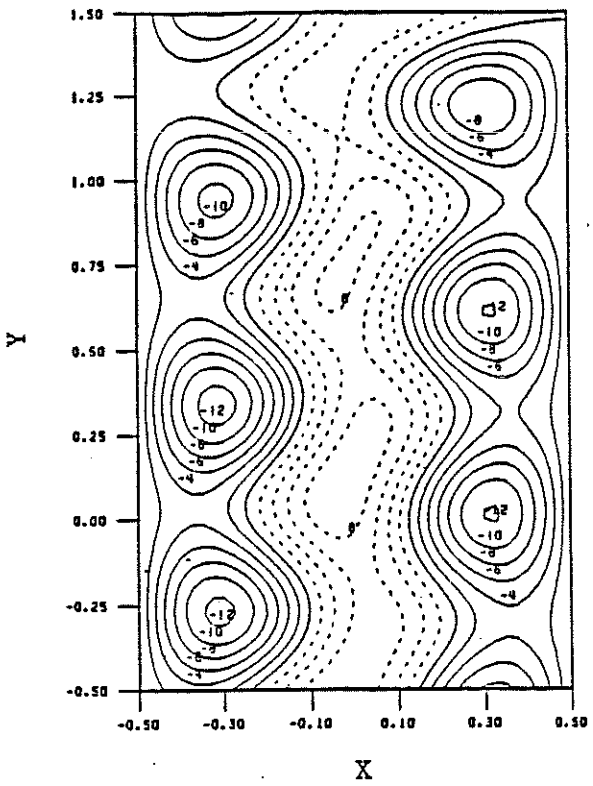

T = 0.14

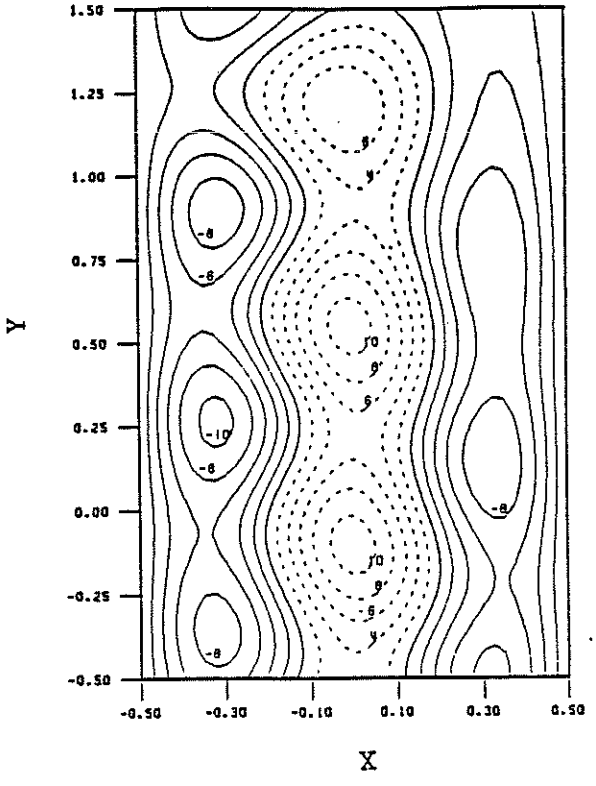

T =0.28

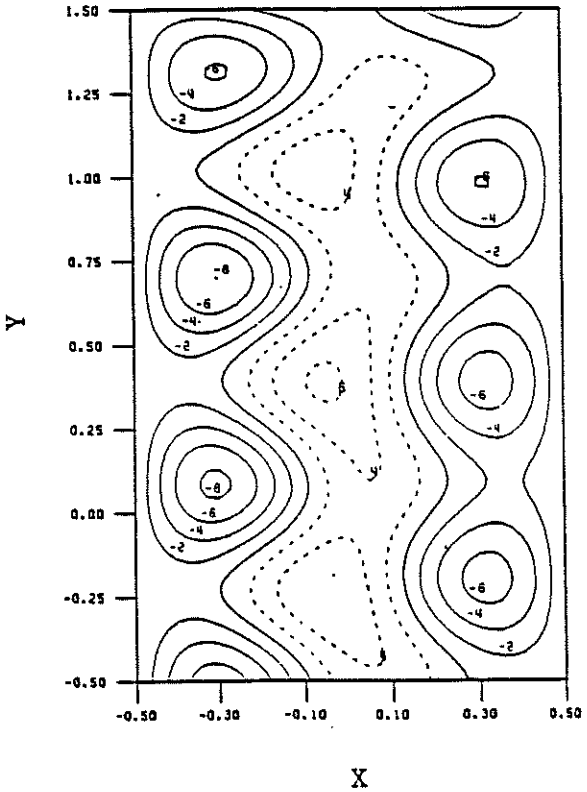

T = 0.42

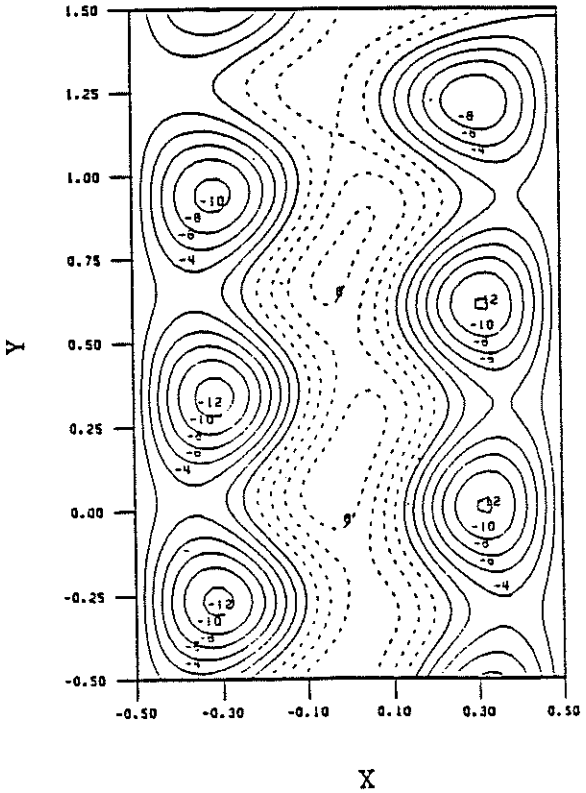

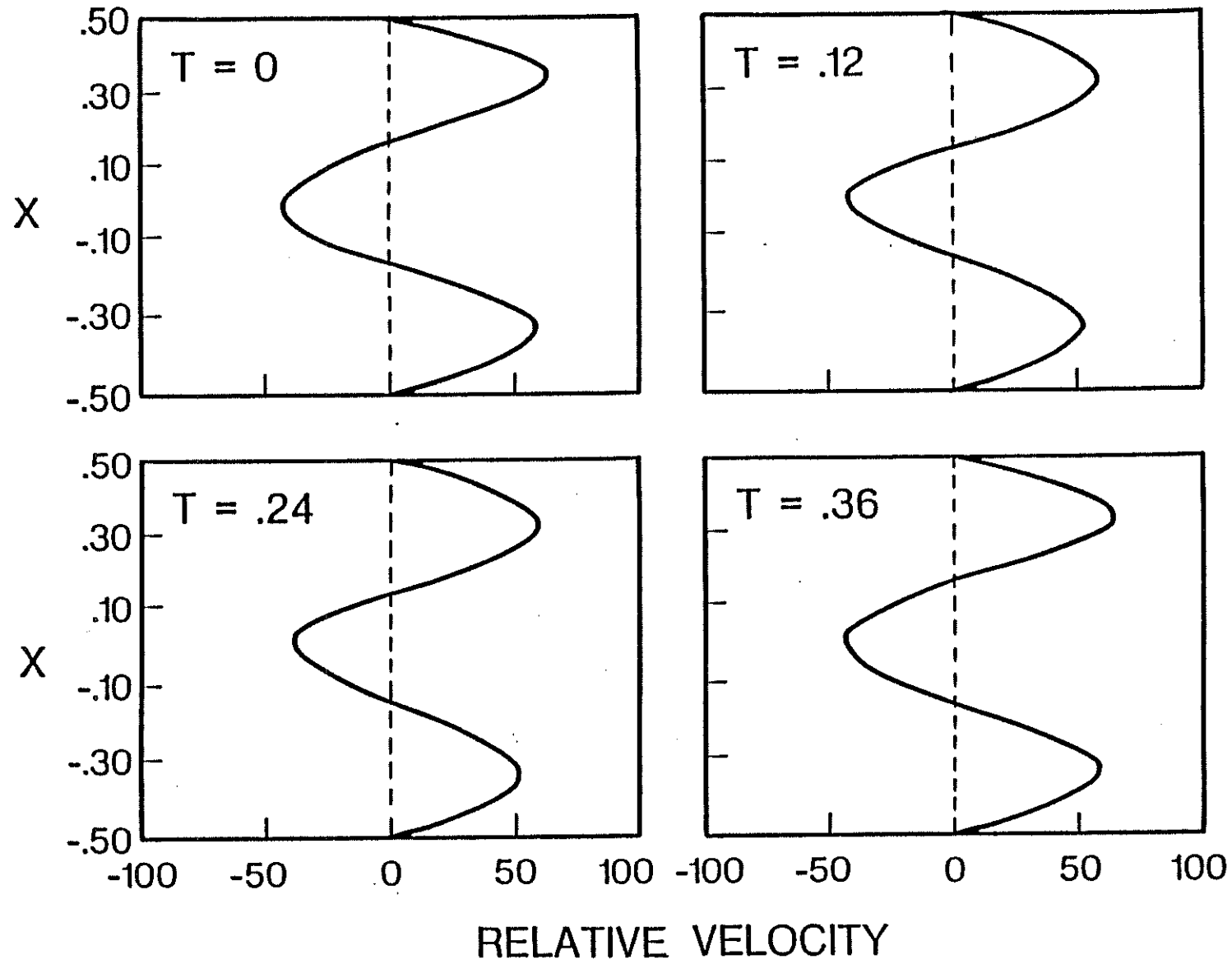
T = 0
T = .12
T = .24
T = .36
.50
.30
.10
-.10
-.30
-.50
X
-100
-50
0
50
100
RELATIVE VELOCITY

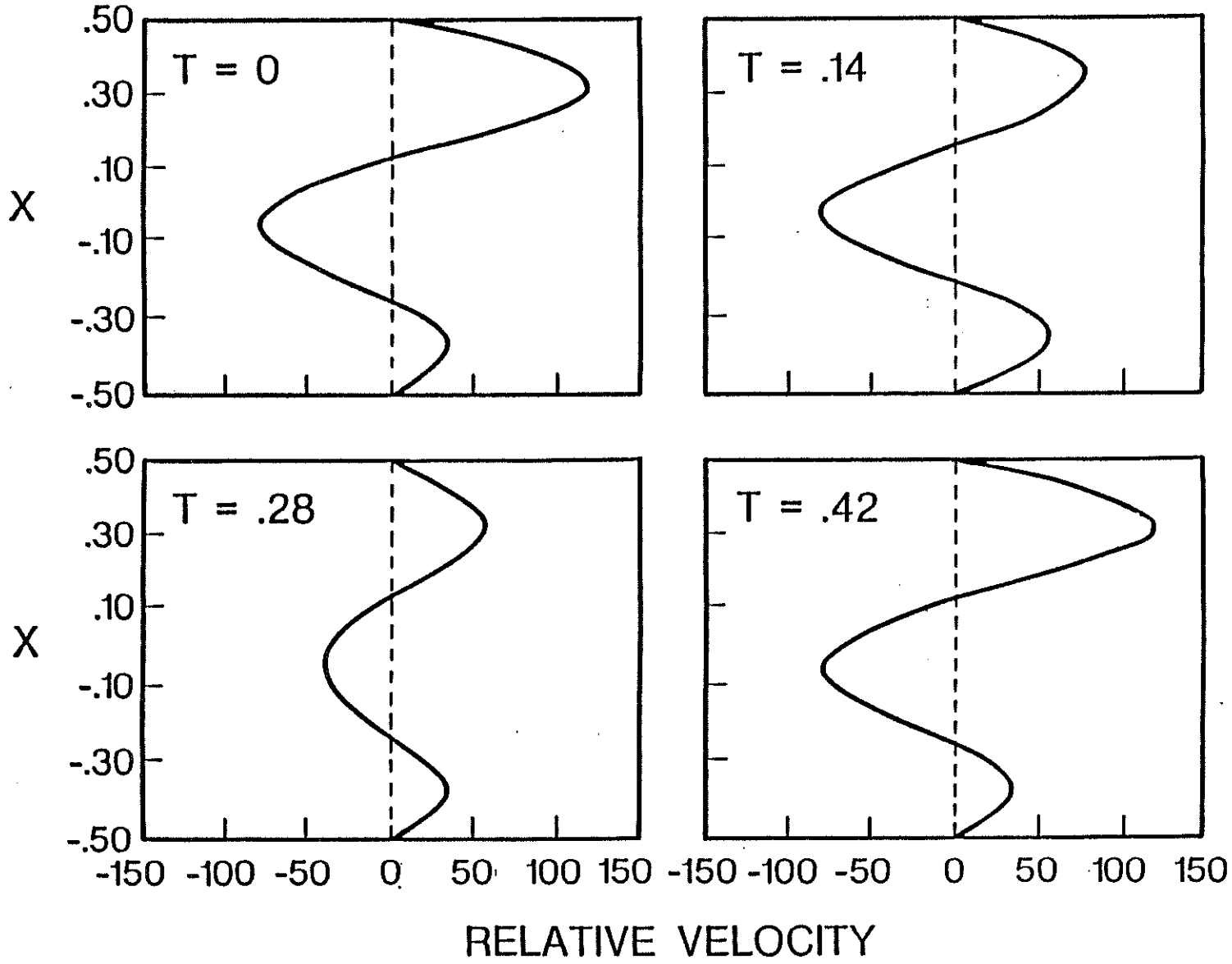
T = 0
T = .14
T = .28
T = .42
.50
.30
.10
-.10
-.30
-.50
X
-150 -100 -50 0 50 100 150
RELATIVE VELOCITY

SOLUTION I

T = 0.0

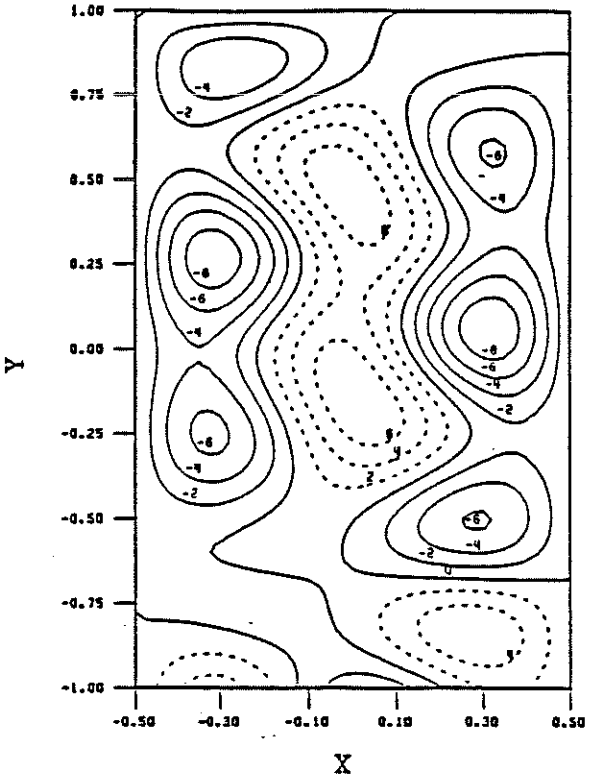

T =0.14

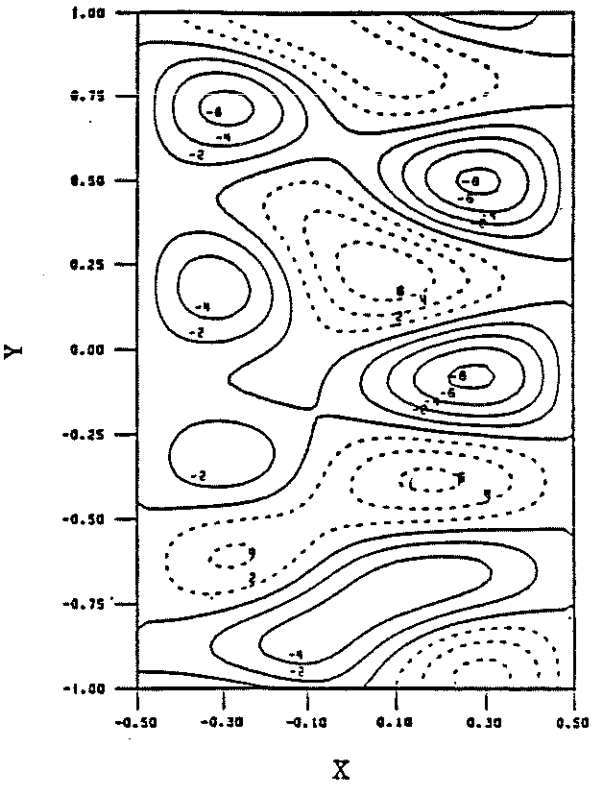

T = 0.28

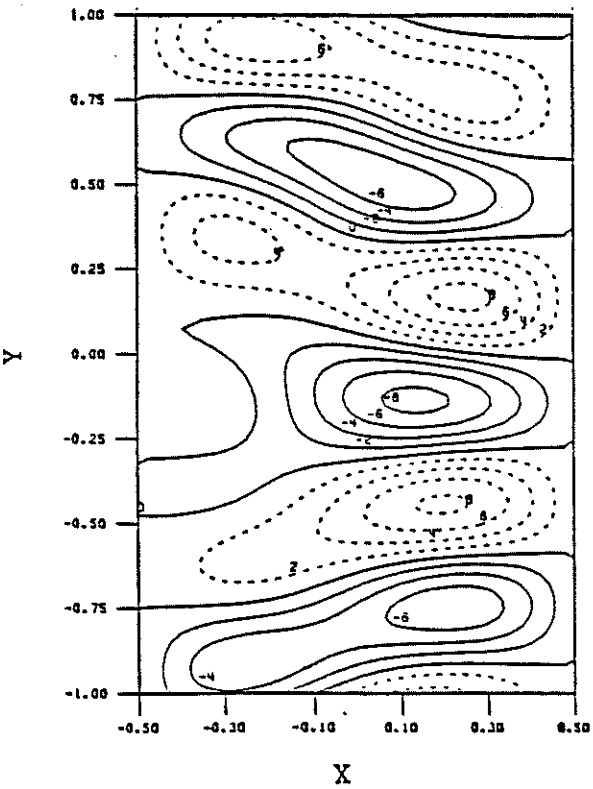

T = 0.42

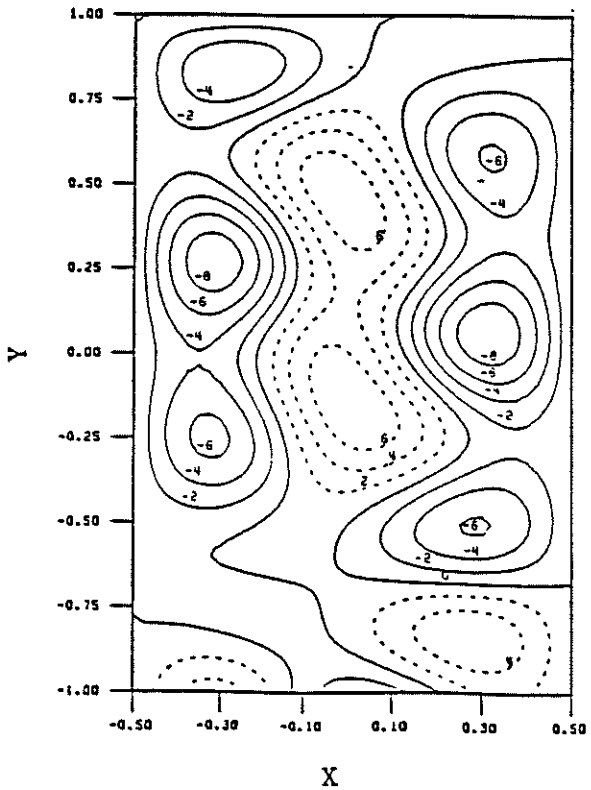

SOLUTION II

T = 0.0

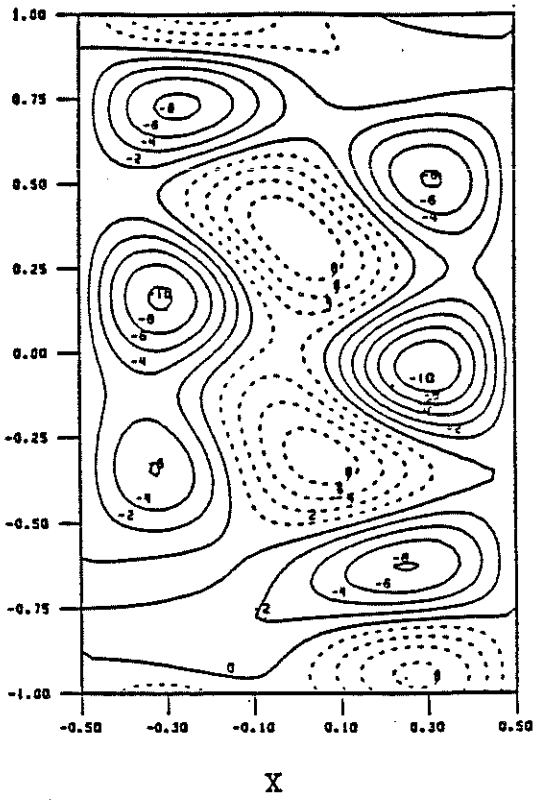

T = 0.18

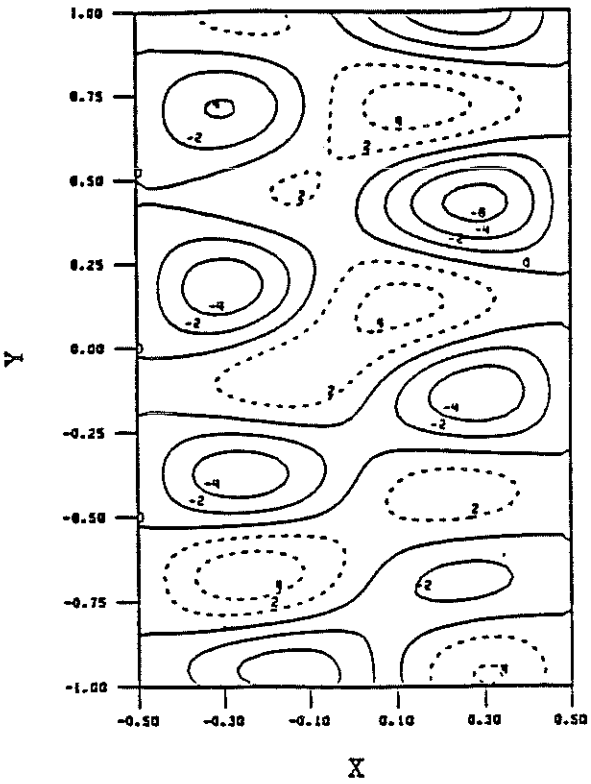

T = 0.36

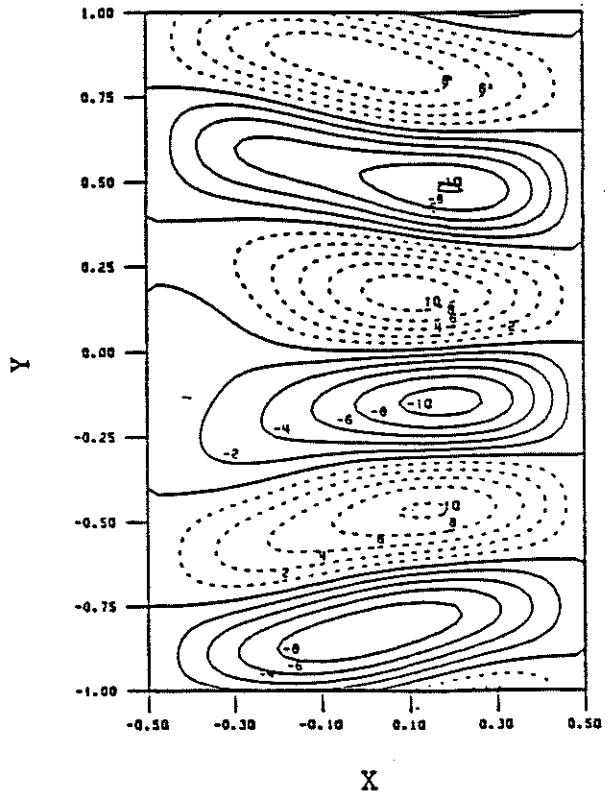

T = 0.54

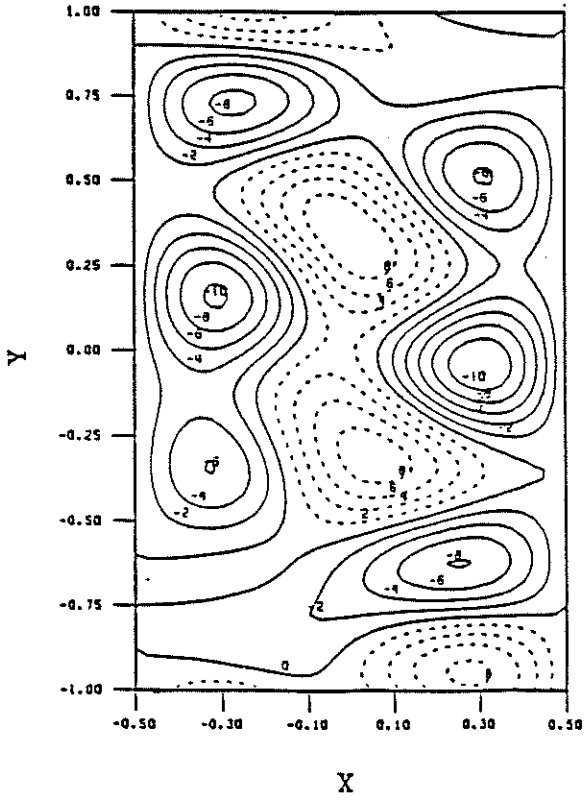

Table I: Critical and Higher Bifurcation Points for Solution I

Wave Number	N_T	B_s	B_d	B_q	B_8	B_{16}	B_a
$\alpha_{(1)} = \alpha_c$ $\alpha_{(2)} = 1.1\,\alpha_c$	4	35836.86	37932.03	38368.01	38459.56	38478.86	38482.56
$\alpha_{(1)} = \alpha_c$ $\alpha_{(2)} = 1.1\,\alpha_c$ $\alpha_{(3)} = 0.1\,\alpha_c$	6	37201.11	40378.25	40967.33	41085.94	41110.49	41129.07
$\alpha_{(1)} = \alpha_c$ $\alpha_{(2)} = 1.2\,\alpha_c$ $\alpha_{(3)} = 0.2\,\alpha_c$	6	38020.02	41201.86	41825.83	41953.36	41980.58	41986.46

Table II: Critical and Higher Bifurcation Points for Solution II

Wave Number	N_T	B_s	B_d	B_q	B_8	B_{16}	B_{qu}	B_a
$\alpha_{(1)} = \alpha_c$ $\alpha_{(2)} = 1.1\,\alpha_c$	4	36303.08	37893.78	38205.23	38271.62	-	38285.41	67681.25
$\alpha_{(1)} = \alpha_c$ $\alpha_{(2)} = 1.1\,\alpha_c$ $\alpha_{(3)} = 0.1\,\alpha_c$	6	37533.63	40597.21	41154.23	41263.45	41286.20	-	41291.04
$\alpha_{(1)} = \alpha_c$ $\alpha_{(2)} = 1.2\,\alpha_c$ $\alpha_{(3)} = 0.2\,\alpha_c$	6	38426.65	41551.31	42109.29	42223.16	42246.64	-	42251.70

Table III: Universal Values of Qn

Solition I

Wave Number	N_T	Q_1	Q_2	Q_3
$\alpha_{(1)} = \alpha_c$ $\alpha_{(2)} = 1.1\,\alpha_c$	4	4.81	4.76	4.74
$\alpha_{(1)} = \alpha_c$ $\alpha_{(2)} = 1.1\,\alpha_c$ $\alpha_{(3)} = 0.1\,\alpha_c$	6	5.39	5.00	4.80
$\alpha_{(1)} = \alpha_c$ $\alpha_{(2)} = 1.2\,\alpha_c$ $\alpha_{(3)} = 0.2\,\alpha_c$	6	5.10	4.89	4.68

Solution II

Wave Number	N_T	Q_1	Q_2	Q_3
$\alpha_{(1)} = \alpha_c$ $\alpha_{(2)} = 1.1\,\alpha_c$	4	5.11	4.69	-
$\alpha_{(1)} = \alpha_c$ $\alpha_{(2)} = 1.1\,\alpha_c$ $\alpha_{(3)} = 0.1\,\alpha_c$	6	5.50	5.10	4.80
$\alpha_{(1)} = \alpha_c$ $\alpha_{(2)} = 1.2\,\alpha_c$ $\alpha_{(3)} = 0.2\,\alpha_c$	6	5.60	4.90	4.85